Environmental Science and Pollution Research (2024) 31:41032–41045
https://doi.org/10.1007/s11356-024-33820-x

RESEARCH ARTICLE

Preparation of composites with MgAl-LDH-modified commercial activated carbon for the quick removal of Cr(VI) from aqueous solutions

Ying Sun[1] · Zexu Wang[1] · Shijie Zhang[1] · Chuyin Liu[1] · Yunfeng Xu[1]

Received: 15 March 2024 / Accepted: 21 May 2024 / Published online: 6 June 2024

Abstract
The problem of soil and water contamination caused by Cr(VI) discharged from the dyeing, electroplating, and metallurgical industries is becoming increasingly serious, posing a potentially great threat to the environment and public health. Therefore, it is crucial to develop a fast, efficient, and cost-effective adsorbent for remediating Cr-contaminated wastewater. In this work, MgAl-LDH/commercial-activated carbon nanocomposites (LDH-CACs) are prepared with hydrothermal. The effects of preparation and reaction conditions on the composite properties are first investigated, and then its adsorption behavior is thoroughly explored. Finally, a potential adsorption mechanism is proposed by several characterizations like SEM–EDS, XRD, FTIR, and XPS. The removal of Cr(VI) reaches 72.47% at optimal conditions, and the adsorption study demonstrates that LDH-CAC@1 has an extremely rapid adsorption rate and a maximum adsorption capacity of 116.7 mg/g. The primary removal mechanisms include adsorption-coupled reduction, ion exchange, surface precipitation, and electrostatic attraction. The reusability experiment illustrates that LDH-CAC@1 exhibits promising reusability. This study provides an effective adsorbent with a remarkably fast reaction, which has positive environmental significance for the treatment of Cr(VI) wastewater.

Keywords Adsorption · Layered double hydroxide · Activated carbon · Cr(VI) · Hydrothermal · LDH-CAC

Introduction

In the past decades, humans have benefited greatly from rapid economic development, as well as frantically destroying the environment indiscriminately (Gholami et al. 2020b). Of these, the pollution of water and soil caused by Cr, a heavy metal emitted from industries like dyeing, leather tanning, and metallurgy, is particularly serious. Cr pollution is also widespread in China. It was listed by the government as one of the most contaminated pollutants (Yang et al. 2019; Zhao et al. 2015). Pessimistically, Cr entering the environment cannot be biodegradable (Gong et al. 2017; Xue et al. 2018). Therefore, it will continuously endanger human health through bioaccumulation and biomagnification as soon as Cr pollution forms (Ali et al. 2022; Wang et al. 2020). In general, Cr exists mainly in the form of Cr(III) and Cr(VI). Among them, Cr(III) is one of the essential trace elements for the human body with low toxicity and poor mobility, which usually exists within the environment in the form of $Cr(OH)_3$ or Cr_2O_3. Conversely, Cr(VI) is highly toxic and mobile and usually exists within the environment in the form of CrO_4^{2-} and $Cr_2O_7^{2-}$, which can damage the kidneys, liver, and other organs in the human body. Consequently, it is essential to implement effective measures to remove Cr(VI) from wastewater. Several techniques have been explored for this purpose, including adsorption, chemical precipitation, ion exchange, and membrane separation (Gossuin et al. 2020; Yaseen et al. 2021; Ye et al. 2019). Among these techniques, adsorption has received significant attention due to its high efficiency, low cost, simplicity of operation, and practicality (He et al. 2020; Yin et al. 2017).

Layered double hydroxide (LDH) is a metal-based nanomaterial with a layered structure that has gained significant

Responsible Editor: Tito Roberto Cadaval Jr

✉ Yunfeng Xu
yfxu@shu.edu.cn

[1] School of Environmental and Chemical Engineering, Shanghai University, No. 99 Shangda Road, Shanghai 200444, China

attention as an emerging adsorbent in recent years. Its general molecular formula is as follows:

$$\left[M_{1-X}^{2+}M_{X}^{3+}(OH)_2\right]^{X+}(A^{n-})_{x/n}\cdot mH_2O$$

where M^{2+} is a divalent metal cation and M^{3+} is a trivalent metal cation; A^{n-} denotes the interlayer anion and n^- represents its charge number. x is the molar fraction (Dong et al. 2022). The unique layered structure of LDH is responsible for its high porosity and large number of exchangeable anions, which leads to favorable adsorption properties along with biocompatibility and cost-effectiveness of LDH. However, LDH particles at the nanoscale are extremely prone to agglomeration, which significantly reduces their adsorption properties. To address this issue, many scholars have attempted to combine LDH with other materials. De Geest et al. prepared composites of MgAl-LDH/bentonite by combining LDH with bentonite. The results indicate that the maximum adsorption capacity of Cr^{3+} and Cr^{6+} is 48 mg/g and 40 mg/g, respectively (De Geest et al. 2023). Liang et al. produced MgAl-LDH/BC-SA aerogels. Compared to LDH nanosheets, the removal efficiency of Cu^{2+} and Cd^{2+} was enhanced by 35% and 41%, respectively (Liang et al. 2023). Moreover, LDH can be combined with various carbon-based materials (e.g., graphene (Nayak and Parida 2019, Zhang et al. 2017)), carbon nanotubes (Bhuvaneswari et al. 2021; Jia et al. 2016), carbon fibers (Fang et al. 2019; Peng et al. 2018), and activated carbon (Gholami et al. 2020a).

Combining LDH with activated carbon (AC) is considered a promising technology. On the one hand, AC has a large specific surface area, providing numerous active sites for LDH to reduce agglomeration. On the other hand, synergistic effects between LDH and AC can also be generated to strengthen pollutant removal, as detailed in the study of Fang et al. (2021). Most studies on LDH-CAC composites currently focus on antibiotics, dyes, and phosphorous removal. However, oxyanion removal and inter anion interactions, as well as feasibility in engineering applications, still need to be fully investigated.

This work presents a nanostructured material prepared from commercial activated carbon loaded with MgAl-LDH for the removal of Cr(VI) from wastewater. The study aims to achieve the following objectives: (i) synthesize LDH-CAC using a simple two-step hydrothermal method; (ii) investigate the adsorption properties and behaviors of LDH-CAC for the removal of Cr(VI); and (iii) propose a potential mechanism for the removal of Cr(VI) by LDH-CAC.

Materials and methods

Chemicals

$MgCl_2{\cdot}6H_2O$ is acquired from Aladdin (Shanghai, China); $AlCl_3{\cdot}6H_2O$, $K_2Cr_2O_7$, H_2SO_4, HNO_3, and NaOH are purchased from Sinopharm Chemical Reagent Co., Ltd. (Shanghai, China). All chemical reagents used in this study are analytical grade and all chemical solutions are prepared using deionized water. Commercial activated carbon (CAC-101, CAC-102, CAC-103) were obtained from Carbon Erno (Henan, China).

Preparation of LDH-CAC composites

The synthesis of LDH-CAC composites is as follows: $MgCl_2{\cdot}6H_2O$ and $AlCl_3{\cdot}6H_2O$ are dissolved in a beaker containing 20 mL of deionized water at a molar mass ratio of 3:1. Then, 2.0 g of urea (CH_4N_2O) is weighed and dissolved in the prepared mixed metal solution. The LDH precursor solution is mixed completely with urea, and commercial activated carbon slurry (prepared by dissolving 1.0 g, 2.0 g, and 3.0 g of CAC-103 in deionized water, respectively) is added and stirred in the magnetic stirrer for 30 min. The mixture is transferred to a Teflon-lined reactor and heated at 180 ℃ for 6 h. After completion of the reaction, the reactor is allowed to cool to room temperature. The resulting product is then centrifuged and washed with deionized water until the pH is almost neutral. Finally, the sample is dried in an oven at 105 ℃ to obtain the LDH-CAC composites, which are named LDH-CAC@1, LDH-CAC@2, and LDH-CAC@3, respectively. In contrast, MgAl-LDH is synthesized without the use of activated carbon.

Characterization

The morphology of the CAC-103, MgAl-LDH, LDH-CAC@1, LDH-CAC@1-Cr is observed by Gemini SEM 300 scanning electron microscope and EDS is used to measure the elemental content of the samples (SEM–EDS). Braeuer-Emmett-Teller (BET) surface area is calculated at 77 K with N_2 adsorption–desorption on Autosorb-IQ2 fully automated Specific Surface Area and Microporous Analyzer. X-ray diffraction spectroscopy (XRD) is carried out on diffractometer with Cu-Kα radiation, with 2θ between 10 and 80°. XRD diffractograms are subsequently analyzed using Jade software to determine sample phases by comparison with a standard card library. The Fourier transform infrared (FTIR) spectra is performed utilizing

the KBr particle method. X-ray photoelectron spectroscopy (Thermo Scientific K-Alpha + , USA) is applied to identify the elemental valence states of the LDH-CAC@1, LDH-CAC@1-Cr (XPS). Zeta potentials are obtained via potentiometric methods.

Experiment of CAC modification

Ten grams of commercial activated carbon (CAC-101, CAC-102, CAC-103) is weighed and placed in a 200-mL beaker. The carbon is then reacted with 10% H_2SO_4 at a solid–liquid ratio of 1:10 (g/mL) for 6 h at room temperature. After the reaction is complete, the mixture is separated into solid and liquid components. The solid is washed continuously with deionized water to maintain a near-neutral pH. Ultimately, the acidified commercial activated carbon is dried in a 105 ℃ oven until constant weight and named as SAC-101, SAC-102, and SAC-103, respectively.

Batch adsorption experiments

At room temperature, 0.1 g of adsorbent (CAC,MgAl-LDH,LDH-CAC) is added to 50 ml of Cr(VI) solution with a concentration of 100 mg/L. The centrifuge tubes are then placed in a thermostatic shaking chamber and left for 6 h. Once the reaction is completed, the concentration of Cr(VI) in the solution was estimated using inductively coupled plasma-atomic emission spectrometer (ICP-OES). To investigate the effect of CAC loading, we set the loadings at 1.0 g, 2.0 g, and 3.0 g. To examine the effect of pH, 1 M HNO_3 and 1 M NaOH are used to adjust the initial pH of the Cr(VI) solution, which was removed as described in the experimental steps above. It is important to note that, in order to investigate the practical usability of LDH-CAC composites, all remaining experiments do not adjust their pH.

The LDH-CAC composites of this work are evaluated using removal efficiency and adsorption capacity. Cr(VI) removal efficiency (%) is calculated as follows:

$$R\% = \frac{C_0 - C_e}{C_0} \times 100\% \tag{1}$$

The adsorption capacity (mg/g) was calculated as follows:

$$q_m = \frac{\left(C_0 - C_e\right) \times V}{m} \tag{2}$$

where C_0 and C_e are the initial and equilibrium concentrations of Cr(VI) (mg/L), respectively; V is the volume of solution (L); m is the mass of adsorbent (g). Three parallel samples were prepared for all experiments, and the errors in the experimental data were expressed as mean deviations.

Kinetic study

To study the adsorption kinetics of LDH-CAC@1, 0.1 g of the composite is used to remove 50 mL of Cr(VI) solution with a concentration of 100 mg/L at room temperature. Samples are taken at specific time intervals (1st, 3rd, 5th, 10th, 15th, 30th, 60th, 150th, 300th, 720th, 1440th min) and the concentration of Cr(VI) in the solution was measured. The results are fitted utilizing both the pseudo-first-order kinetic model (PFO) and the pseudo-second-order kinetic model (PSO):

Pseudo-first-order kinetic model (PFO):

$$\frac{dq_t}{q_t} = k_1\left(q_e - q_t\right) \tag{3}$$

Transform into:

$$q_t = q_e\left(1 - e^{-k_1 t}\right) \tag{4}$$

Pseudo-second-order kinetic model (PSO):

$$\frac{dq_t}{q_t} = k_2\left(q_e - q_t\right)^2 \tag{5}$$

Transform into:

$$q_t = \frac{k_2 q_e^2 t}{1 + k_2 q_e t} \tag{6}$$

In the formula, q_e and q_t (mg/g) represent the amount of Cr(VI) adsorbed at equilibrium and time t (min), respectively. k_1 and k_2 represent the pseudo-first-order adsorption rate constant (mg/g) and the pseudo-second-order adsorption rate constant ($g \cdot mg^{-1} \cdot min^{-1}$), respectively.

Isotherm study

The batch equilibrium approach is performed to analyze the isothermal adsorption process of Cr(VI) by LDH-CAC@1. Specific procedures are followed: 0.1 g LDH-CAC@1 is weighed and used to remove of 50 mL of Cr(VI) with concentrations ranging from 5 to 1000 mg/L (5, 10, 25, 50, 100, 200, 300, 400, 600, 800, and 1000 mg/L). The concentration of Cr(VI) in the solutions was measured after 24 h of continuous reaction at 298.15 K, 308.15 K, and 318.15 K. The results are then simulated using the Langmuir and Freundlich isotherm adsorption models:

Langmuir isotherm adsorption model:

$$\frac{C_e}{q_e} = \frac{1}{q_{\max} K_L} + \frac{C_e}{q_{\max}} \tag{7}$$

C_e, q_e, and q_{max} respectively represent the concentration of remaining Cr(VI) in the solution, the adsorption capacity, and the maximum adsorption of LDH-CAC@1 during adsorption equilibrium; their units are milligrams/gram. K_L is the adsorption equilibrium constant (L/mg).

Freundlich isotherm adsorption model:

$$\lg\ q_e = \lg\ K_F + \frac{1}{n}\lg\ C_e \tag{8}$$

where C_e and q_e respectively represent the concentration of remaining Cr(VI) in the solution and the adsorption capacity of LDH-CAC@1 during adsorption equilibrium; their units are milligrams/gram. K_F is the adsorption capacity constant in milligrams/gram. n is the Freundlich constant.

Results and discussion

The exploration of LDH-CAC synthesis conditions

Effect of CAC on the removal of Cr(VI) before and after acidification

Acid modification is considered one of the effective ways for enhancing the performance of activated carbon in removing Cr(VI) (Soleimani et al. 2023). Therefore, it is necessary to investigate the impact of acid modification on Cr(VI) removal.

Figure 1a demonstrates the removal efficiency of Cr(VI) before and after modification for three different types of commercial activated carbon. The results show that after acid modification, the Cr(VI) removal of both CAC-101 and CAC-102 has improved by 5.98% and 6.73%, respectively. This improvement can be attributed to the increase in the number of functional groups on the surface of activated carbon after acid modification and the change in surface chemistry (Srivastava et al. 2021). However, the removal efficiency of Cr(VI) by CAC-103 modified rather decreases from 45.35 to 37.95%. This indicates that activated carbons with varying physical and chemical properties respond differently to acid alteration. The decrease in the adsorption capacity of CAC-103 was mainly caused by partial pore wall collapse of the activated carbon due to the oxidizer treatment and pore blockage resulting from the introduction of oxygenated functional groups, which are the main reasons for the decrease in the adsorption capacity of CAC-103 (Shim et al. 2001). Overall, SAC-102 exhibits the highest adsorption capacity for Cr(VI), followed by CAC-103. Overall, SAC-102 exhibited the highest removal of Cr(VI), followed by CAC-103. Considering the economic and practical aspects of engineering, CAC-103 is chosen for future experiments.

Effect of activated carbon loaded

Figure 1b illustrates the impact of activated carbon dosage on the performance of LDH-CAC composites for Cr(VI) removal. The initial removal efficiency of initial Cr(VI) by MgAl-LDH and CAC-103 is poor, with only 21.44% and 42.57%, respectively. In contrast, the LDH-CAC composites (LDH-CAC@1, LDH-CAC@2, and LDH-CAC@3) exhibit better removal, with 65.99%, 48.25%, and 53.59%, respectively. The improvement in removal efficiency can be reasonably explained by the synergistic effect. On the one hand, activated carbon can provide numerous active sites for LDH, preventing agglomeration of LDH particles; on the other hand, LDH can enhance the surface properties of activated carbon and increase its anion exchange capacity. Moreover, the removal efficiency of LDH-CAC decreases with increasing carbon loading, likely due to CAC aggregation at high content, resulting in decreased surface properties (Blaisi et al. 2018). Therefore, LDH-CAC@1 was selected as the optimal ratio for the subsequent experiments.

Effect of initial pH

The impact of initial pH on the adsorption capacity of LDH-CAC@1 for Cr(VI) is frequently discussed due to its effect on the surface properties of LDH-CAC@1, the form of Cr(VI) species, and the ionic state of surface functional groups (Wang et al. 2018, 2022). As shown in Fig. 1c, the

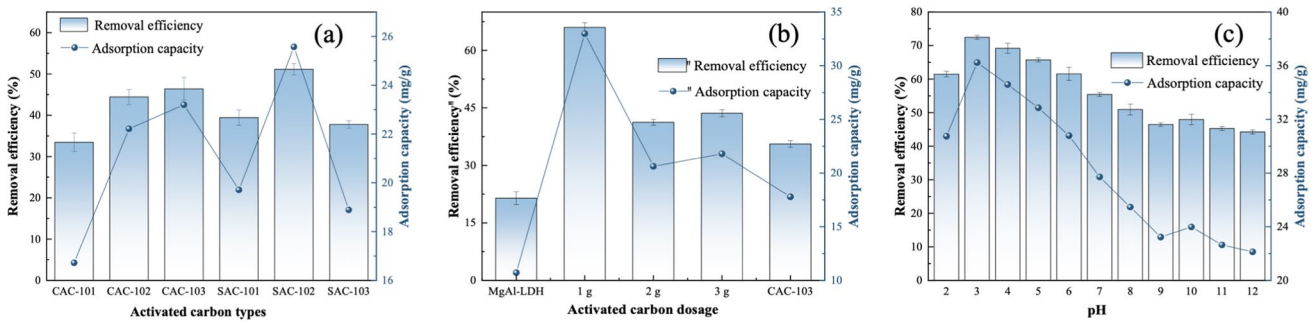

Fig. 1 Effect of acidification (**a**), activated carbon dosage (**b**), and initial pH (**c**) towards Cr(VI) removal performance of LDH-CAC@1

adsorption of Cr(VI) by LDH-CAC@1 initially increases and then decreases with increasing pH, which is consistent with the findings of Huang et al. (2019). The results show that a 72.47% Cr(VI) removal efficiency is achieved at pH 3. The decrease in removal efficiency at higher pH levels may be attributed to the Zeta potential (Fig. 6). Based on the Zeta potential, the surface of the LDH-CAC@1 is consistently positively charged at pH < 8.51, resulting in an electrostatic attraction between LDH-CAC@1 and $Cr_2O_7^{2-}$. However, as the pH decreases, there is an electrostatic repulsion between $Cr_2O_7^{2-}$ and OH^-. As the amount of OH^- in the solution increases, competitive adsorption between the two ions continues, leading to a decline in adsorption performance (Huang et al. 2019).

Characterization

SEM–EDS

Surface morphology was observed by SEM for CAC-103, MgAl-LDH, LDH-CAC@1, and LDH-CAC@1-Cr (Fig. 2). The surface morphology of CAC-103 exhibits a comparatively rough, porous spongy structure with a high surface area of 1145.29 m^2/g (Fig. 2a, b). MgAl-LDH has a slightly smooth surface at low magnification, while irregular crystal

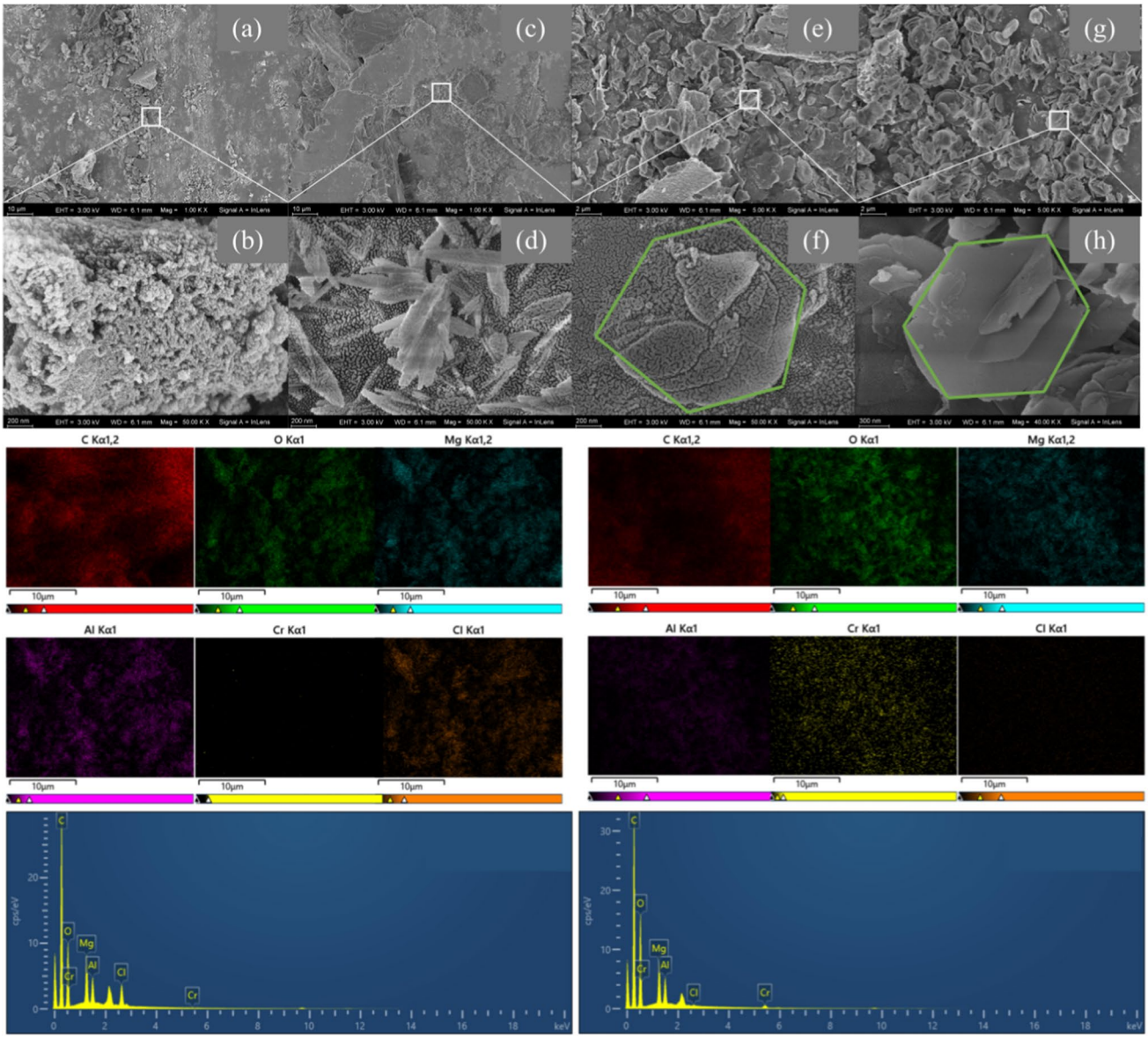

Fig. 2 SEM images of CAC-103 (**a**–**b**), MgAl-LDH (**c**–**d**), LDH-CAC@1 (**e**–**f**), and LDH-CAC@1-Cr. EDS images of LDH-CAC@1 (bottom left), LDH-CAC@1-Cr (bottom right)

morphology is observed at high magnification (Fig. 2c, d). Figure 2e, f show the surface morphology of LDH-CAC@1, which exhibits a larger number of hexagonal lamellae, which are considered the typical structure of LDH. Additionally, the EDS images illustrate uniform distribution of elements such as C, O, Mg, Al, and Cl over the LDH-CAC@1 surface, meaning that LDH-CAC@1 has been successfully prepared. Surface observations of LDH-CAC@1-Cr were performed at the end of adsorption (Fig. 2g, h) and the crystal structure remained intact. The EDS images indicated no significant difference in the C, O, Mg, and Al content before and after adsorption. However, the relative percentage of Cl decreased from 2.32 to 0.11%, and Cr increased from 0.01 to 1.22%. These results demonstrate that Cr(VI) was adsorbed on the LDH-CAC@1. Table 1 shows the semi-quantitative results before and after adsorption.

XRD

The crystal structures of CAC-103, MgAl-LDH, LDH-CAC@1, and LDH-CAC@1-Cr are examined by XRD (Fig. 3a). CAC-103 shows a broad peak at 22.5°,which is typical of an amorphous graphite structure (Sirajudheen et al. 2020). The XRD peaks for MgAl-LDH appear at 11.4°, 22.96°, 34.8°, 39.1°, 46.7°, and 60.6°, representing (003), (006) (012), (015), (018), (110), and (113) planes, respectively (PDF# 35–0965). The intensities remain high, indicating that the samples have a high degree of crystallinity and a typical lamellar structure. The XRD pattern of LDH-CAC@1 shows a reduction in the intensities of the characteristic peaks corresponding to LDH. The decrease in characteristic peak intensity of LDH-CAC@1 may be attributed to the reduction in crystallinity and crystal structure caused by the addition of activated carbon. The interlayer spacing d003 calculated from Bragg's law for (003) crystalline surfaces indicates that the interlayer spacing of LDH-CAC@1 remains the same as that of MgAl-LDH (0.78 nm). This suggests that LDH-CAC@1 also has good crystallinity and crystal structure.

FTIR

The FTIR spectra of CAC-103, MgAl-LDH, LDH-CAC@1, and LDH-CAC@1-Cr are shown in Fig. 3b. Characteristic peaks at 3375 cm^{-1} and 1605 cm^{-1} correspond to hydroxyl groups (O–H) or water molecules in LDH intercalation (Extremera et al. 2012; Ren et al. 2022a). Among them, the highest peak intensity is observed for MgAl-LDH, which is consistent with the XRD spectra. This is followed by LDH-CAC@1, where the decrease in peak intensity is probably correlated with CAC doping. After Cr(VI) adsorption, the intensity of the characteristic peaks decreases again, suggesting that O–H was involved in the process of Cr(VI) removal. This is similar to the change in the O1s peaks of the XPS. The characteristic peaks at 1401 cm^{-1} correspond to C–O or N–O, which can be attributed to the influence

Table 1 Semi-quantitative analysis of LDH-CAC@1 constituent element (%)

Project	Elements					
	C	O	Mg	Al	Cl	Cr
Before	69.58	22.58	3.58	1.94	2.32	0.01
After	62.88	30.13	3.52	2.14	0.11	1.22

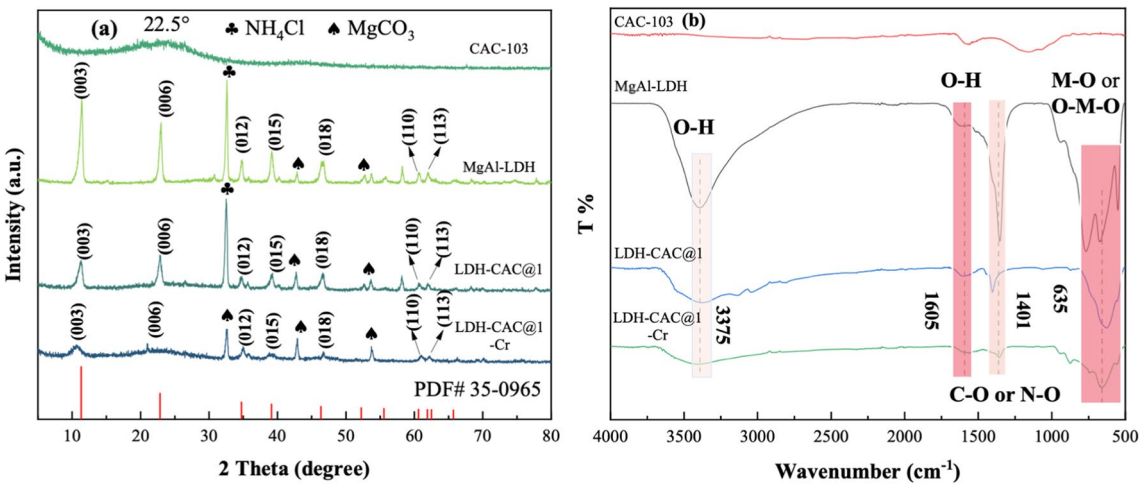

Fig. 3 The XRD patterns (**a**) and FTIR spectra (**b**) of CAC-103, MgAl-LDH, LDH-CAC@1, and LDH-CAC@1-Cr

of CO_2 in the air during the synthesis process, thus causing the stretching vibration of CO_3^{2-} (Gao et al. 2021). The variation in peak intensity is consistent with O–H, which is related to the following factors: (i) continuous ion exchange between CO_3^{2-} and Cr(VI) anion groups in the solution; (ii) direct involvement of C–O in the chemical reaction, which is oxidized to C = O, reducing its intensity. The characteristic peaks around 500–800 cm^{-1} are attributed to the telescopic vibrations of M–O and O–M–O. FTIR spectroscopic results present that LDH-CAC@1 is successfully synthesized.

XPS

To further investigate the chemical properties of LDH-CAC@1, sequential XPS characterization was performed. Figure 4 shows the total spectra of LDH-CAC@1 before and after adsorption. Before adsorption, characteristic peaks corresponding to Mg 1s, O 1s, N 1s C 1s, Cl 2p, and Al 2p appear at 1304.99, 532.95, 399.96, 286.48, 199.08, and 75.37 eV; after Cr(VI) adsorption, in addition to the original characteristic peaks, a new characteristic peak corresponding to Cr 2p also appears at 579.08 eV, indicating that Cr(VI) was successfully adsorbed on LDH-CAC@1. In addition, a significant decrease in the intensity of the characteristic Cl 2p peak after adsorption is also observed, which is consistent with the changes in the EDS images. High-resolution spectral analysis of C 1s, N 1s, and O 1s before and after adsorption reveals that the main changes are observed to be concentrated in C–O, C = O, C–N, C = N, NO_3^-, NO_2^-, O–H, and CO_3^{2-}, respectively. It indicates that these functional groups were directly involved in the chemical reaction and caused changes in its chemical state via oxidation or ion exchange. The XPS spectra of Cr 2p show the presence of both Cr(VI) and Cr(III), indicating that there may have been a reduction during the reaction which changes the valence form of Cr(VI).

N_2 adsorption–desorption curve

The BET isotherm is shown in Fig. 5. Detailed data are given in Table 2. Based on the figures, the specific surface area, average pore size, and total pore volume of CAC-103 are 1145.286 m^2/g, 0.524 nm, and 0.886 cm^3/g, respectively. The large surface area provides many active sites for nano-LDH, helping to prevent agglomeration of nanoparticles. As classified by IUPAC, the adsorption of Cr(VI) by CAC-103 belongs to the type IV adsorption isotherm with H4 hysteresis loop, which is a typical curve for activated carbon. For MgAl-LDH, the parameters are 29.525 m^2/g, 4.887 nm, and 0.055 cm^3/g, respectively. The smaller specific surface area is obviously unfavorable for Cr(VI) adsorption, and the tiny particle sizes also cause agglomeration among nano-LDH particles. The adsorption of Cr(VI) belongs to the type III adsorption isotherm with H3-type hysteresis loop, indicating that a large number of mesopores existed in MgAl-LDH. The LDH-CAC@1 parameter are 416.718 m^2/g, 0.524 nm, and

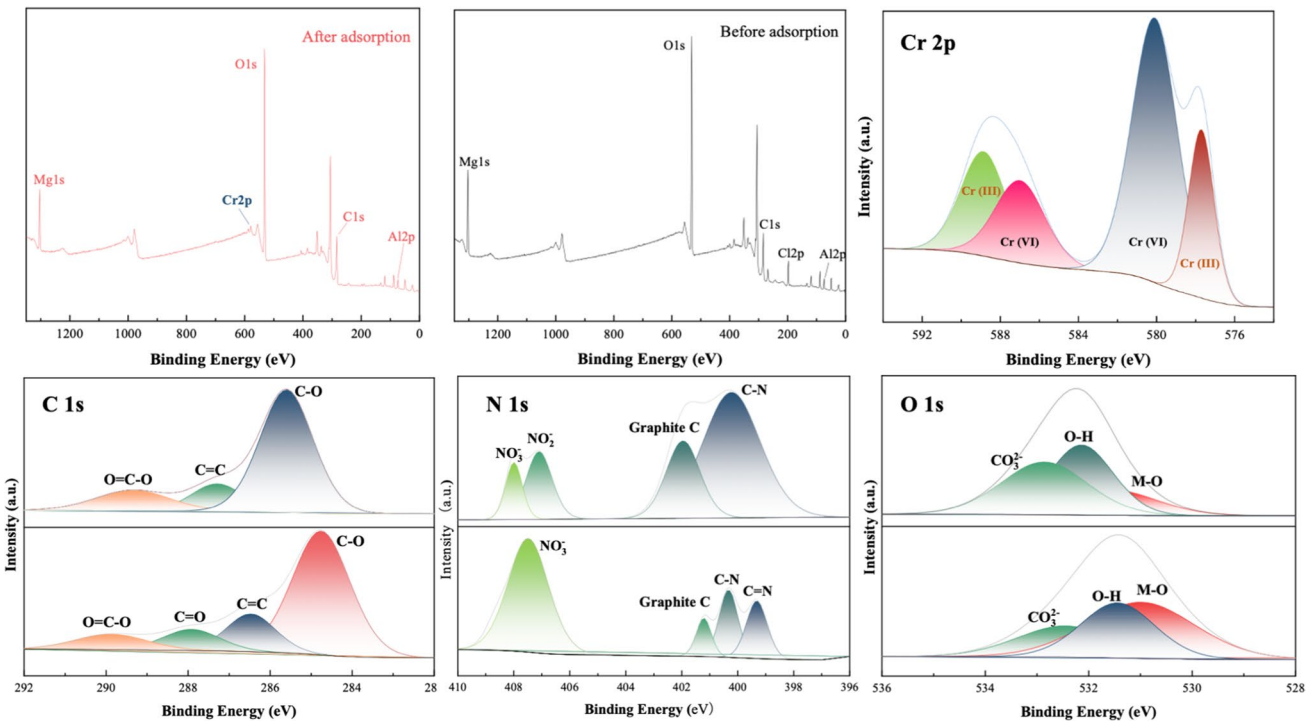

Fig. 4 XPS spectrum analysis of LDH-CAC@1 composite before and after adsorption

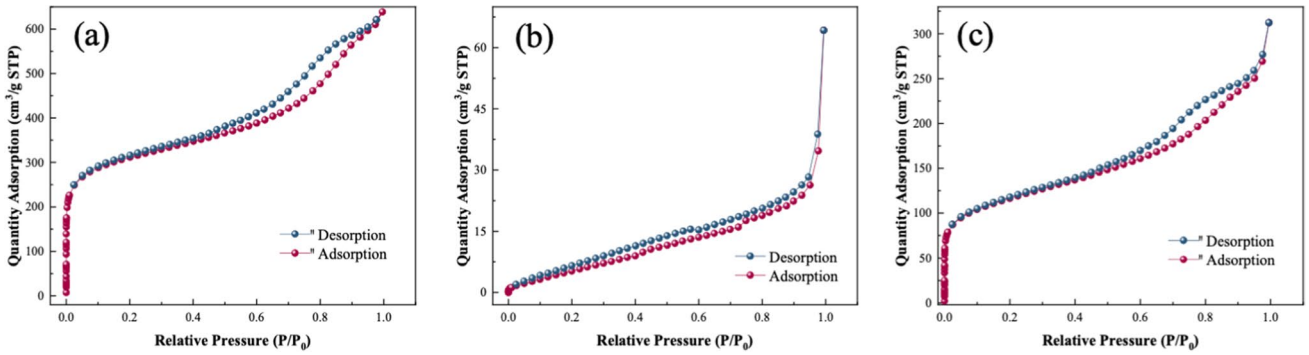

Fig. 5 N_2 adsorption–desorption curves of CAC-103 (**a**), MgAl-LDH (**b**), and LDH-CAC@1 (**c**)

Table 2 N_2 adsorption–desorption isotherms and pore structure parameters of CAC-103, MgAl-LDH, LDH-CAC@1

Samples	BET (m^2/g)	Average pore size (nm)	Total pore volume (cm^3/g)
CAC-103	1145.286	0.524	0.886
MgAl-LDH	29.525	4.887	0.055
LDH-CAC@1	416.718	0.524	0.399

0.399 cm^3/g. Due to the supporting effect of activated carbon, nano-LDH particles could not only reduce interparticle agglomeration, but also bond with active sites on the surface of activated carbon. This greatly improved the pore structure of LDH and facilitated the adsorption performance for Cr(VI). The adsorption of Cr(VI) by LDH-CAC@1 exhibits IV-type adsorption isotherms with H4-type hysteresis loops, which are usually found in some mesoporous zeolite molecular sieves and micro and mesoporous carbon materials. This also indicated that the prepared LDH-CAC@1 possesses both activated carbon and LDH properties.

Zeta potential

According to the morphological changes of Cr(VI), the concentration and pH of the Cr(VI) solution determine the form in which Cr(VI) exists (Lv et al. 2018). At pH < 1, Cr(VI) exists mainly as H_2CrO_4; at 1 < pH < 6.5, Cr(VI) exists mainly as $HCrO_4^-$ and $Cr_2O_7^{2-}$ ions; at pH > 6.5, CrO_4^{2-} ions are the primary form of existence (Wei et al. 2013). The Zeta potential of LDH-CAC@1 is depicted in Fig. 6, and the pH_{pzc} of LDH-CAC@1 is 8.51. As shown in the graph, when the pH of Cr(VI) solution < pH_{pzc}, the surface of LDH-CAC@1 is positively charged and has electrostatic attraction with anions. Conversely, when pH > pH_{pzc}, the surface of LDH-CAC@1 is negatively charged. And LDH-CAC@1 has electrostatic repulsion with anions. As a result, when the pH of the solution is low, LDH-CAC@1 is more easily eliminated by electrostatic attraction with

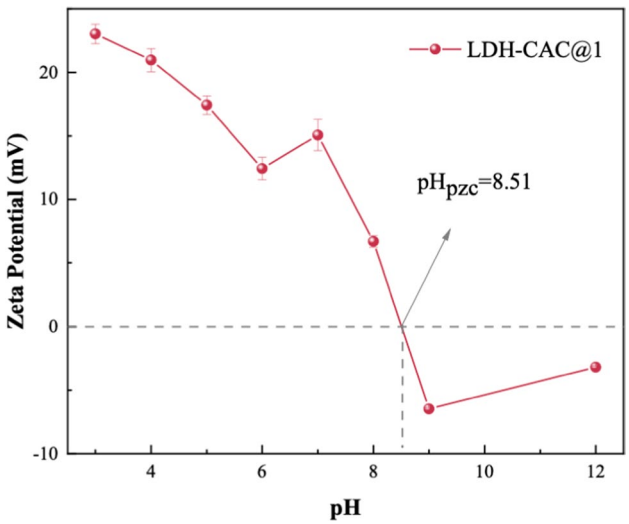

Fig. 6 Zeta potential plots of LDH-CAC@1 (b) at different pH conditions

$HCrO_4^-$,$Cr_2O_7^{2-}$, and CrO_4^{2-} (Lv et al. 2018). However, the charge on the surface of LDH-CAC@1 becomes negative as the pH increases. Its interaction with the Cr(VI) anion changes to electrostatic repulsion. As a result, the adsorption performance of LDH-CAC@1 on Cr(VI) decreases, which can be confirmed in Fig. 1 c.

Adsorption behavior studies

Adsorption kinetics

The adsorption kinetics of LDH-CAC@1 are shown in Fig. 7. The adsorption capacity of LDH-CAC@1 for Cr(VI) increases rapidly with time and reaches adsorption equilibrium in a remarkably short period of time (10 min). PFO kinetic and PSO kinetic models are used for fitting and the corresponding parameters are listed in Table 3. Based on R^2 (R^2 = 0.980), it is concluded that the adsorption process of LDH-CAC@1 is more consistent with the PSO kinetic

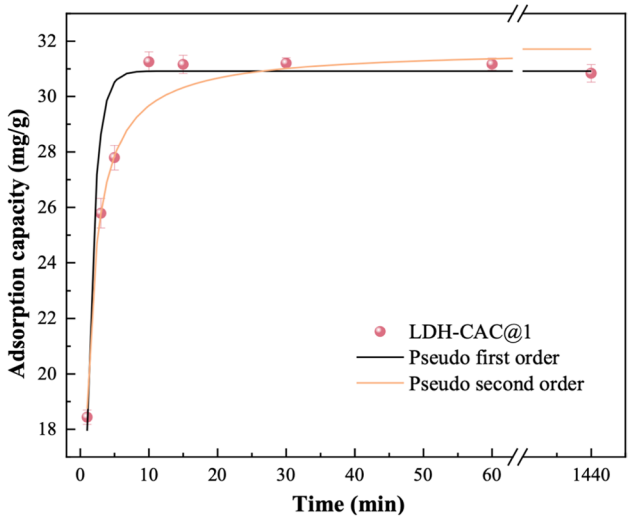

Fig. 7 Pseudo-first-order and pseudo-second-order kinetic models for Cr(VI) adsorption on LDH-CAC@1

Table 3 Parameters related to adsorption kinetics of pseudo-first-order and pseudo-second-order kinetic models

Model	Parameters	LDH-CAC@1
Pseudo-First-Order kinetic	q_e	30.918
	k_L	0.869
	R^2	0.965
Pseudo Second-Order kinetic	q_e	31.728
	k_L	0.045
	R^2	0.980

model, which implies that the adsorption of Cr(VI) is dominated by chemisorption.

Adsorption isotherms

Using the Langmuir, Freundlich models to fit the data, the corresponding parameters are shown in Table 4. It could be seen that the Freundlich isotherm model ($R^2 > 0.978$) fitted the adsorption process better than the Langmuir isotherm model ($R^2 > 0.938$). And the K_F value increased with increasing temperature, indicating that the rising temperature was favorable for the reaction to occur. $0 < 1/n < 1$ indicated that it was conducive to the adsorption process and the reaction was easy to occur. However, the difference in R^2 between the two isotherms was not significant, suggesting that the removal of LDH-CAC@1 may involve multiple adsorptions. Moreover, the maximum adsorption capacity of LDH-CAC@1 was 116.647 mg/g according to the fitting results of the Langmuir model, which agreed with the experimental results (Fig. 8).

Adsorption thermodynamics

The thermodynamic analysis of LDH-CAC@1 was carried out on the basis of adsorption isotherms (Fig. 9). A straight line was fitted with 1/T as the horizontal coordinate and Ln_{KF} as the vertical coordinate. The slope and intercept of the fitted line were calculated as ΔH and ΔS in Eq. 9, and then as ΔG in Eq. 10. The detailed calculation results are summarized in Table 5.

$$LnK_F = -\frac{\Delta H}{RT} + \frac{\Delta S}{R} \tag{9}$$

$$\Delta G = -RTLnK_F \tag{10}$$

As shown in Table 5, the enthalpy (ΔH) was 26.63 kJ/mol > 0, indicating that the adsorption process of Cr(VI) by LDH-CAC@1 was an endothermic process. Increasing temperature is favorable to the reaction, consistent with the trend of isotherms. The entropy (ΔS) was 104.47 kJ/mol > 0 in the adsorption process, demonstrating that the ΔS of the system enhanced as the adsorption reaction continued. This meant that the disorder of the system was raised after the adsorption of Cr(VI) by LDH-CAC@1. The Gibbs free energies (ΔG) of the adsorption process were − 4.544, − 5.516, and − 6.636 kJ/mol at temperatures of 298 K, 308 K, and 318 K, respectively. $\Delta G < 0$, suggesting that the adsorption of Cr(VI) by LDH-CAC@1 was spontaneous. Furthermore, the absolute value of ΔG progressively grew with increasing temperature, similarly implying that the adsorption was more efficient at high temperatures.

Table 4 Parameters related to Langmuir and Freundlich isotherms

Model	Parameters	LDH-CAC@1					
		298 K	CK	308 K	CK	318 K	CK
Langmuir	q_{max}	110.192	95.765	114.003	99.977	116.647	105.344
	K_L	0.0085	/	0.010	/	0.011	/
	R^2	0.990	/	0.955	/	0.938	/
Freundlich	K_F	6.253	/	8.612	/	12.292	/
	$1/n$	0.421	/	0.326	/	0.378	/
	R^2	0.981	/	0.988	/	0.978	/

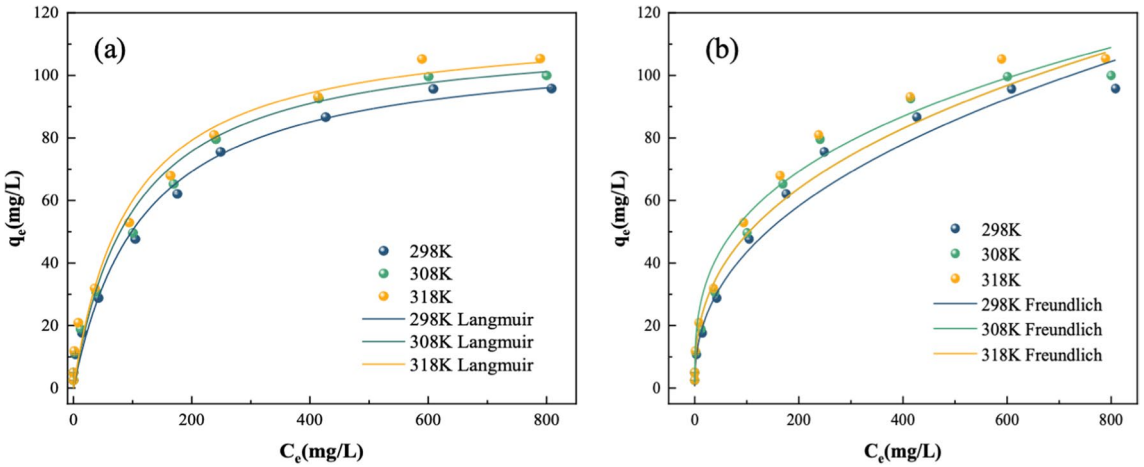

Fig. 8 Langmuir (**a**) and Freundlich (**b**) isotherms for Cr(VI) on LDH-CAC@1

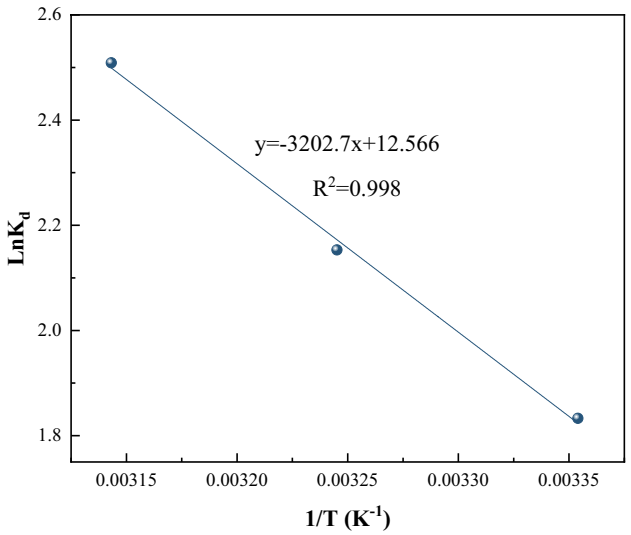

Fig. 9 Thermodynamics study of LDH-CAC@1

Table 5 The thermodynamic parameters of LDH-CAC@1

Temperature (K)	Thermodynamic parameters		
	ΔG (kJ/mol)	ΔH (kJ/mol)	ΔS (J/mol K)
298.15	−4.544	26.63	104.47
308.15	−5.516		
318.15	−6.636		

Mechanisms

A mechanism for the removal of Cr(VI) by LDH-CAC@1 is proposed and better understood by spectroscopic techniques such as Fourier transform infrared spectroscopy (FTIR), X-ray diffraction (XRD), and X-ray photoelectron spectroscopy (XPS). It mainly involves interlayer ion exchange, surface precipitation, adsorption coupled reduction, and electrostatic attraction.

The interlayer anion in the synthesis of LDH-CAC@1 is mainly CO_3^{2-} due to the influence of CO_2 in the air. This means that the XRD and XPS O 1s spectra of LDH-CAC@1 both show the presence of CO_3^{2-}. After the adsorption of Cr(VI), $MgCO_3$ replaced the crystal structure corresponding to NH_4Cl, and the area of the prominent peaks in the O 1s spectra related to CO_3^{2-} decreases significantly. It also means that an ion-exchange interaction occurs between LDH-CAC@1 and Cr(VI) anions by releasing interlayer CO_3^{2-} ions during the reaction process (Gao et al. 2020; Hudcová et al. 2022). In addition, semi-quantitative examination of EDS profiles and elements before and after adsorption shows that the relative mass percentage of Cl^- decreases from 2.32 to 0.11%, while that of Cr increases from 0.01 to 1.22%. Assuming that Cl^- also plays a role in the elimination of Cr(VI), the reaction process can be denoted by Eq. (11) (Yue et al. 2017). The Cl^- releases into solution, and then reacts with OH^- and Mg^{2+} in solution to form $Mg_2Cl(OH)_3$ precipitate, which is deposited on the surface of LDH-CAC@1. The reaction process can be described by Eq. (12) (Yue et al. 2017).

$$Cr(VI) + Cl - LDH \rightarrow Cr(VI) - LDH + Cl^- \quad (11)$$

$$Cl^- + 2Mg^{2+}6H_2O \rightarrow Mg_2Cl(OH)_3 + 3H_3O^+ \quad (12)$$

Moreover, the removal of Cr(VI) is also aided by numerous oxygen-containing functional groups on the surface of LDH-CAC@1. In the FTIR spectra, a significant decrease in the intensity of –OH at 3375 cm^{-1} and 1605 cm^{-1} is observed. In the O 1s spectra, the intensity of the O–H peak also decreases while the intensity of the M–O peak increases

significantly. It means that functional groups result in the continuous formation of metal-containing oxides on the surface of LDH-CAC@1 (Gao et al. 2020; Wang et al. 2016). Meanwhile, the Cr 2p mapping reveals the distinctive peaks associated with Cr(III). This phenomenon can be explained by observing the spectral changes of C 1s and N 1s before and after adsorption. In the C 1s spectra, part of C–O is oxidized to C = O and Cr(VI) is reduced to Cr(III); in the N 1s spectra, C–N follows a similar pattern to C–O and all the NO_2^- is converted to NO_3^- after Cr(VI) adsorption (Tran et al. 2019).

In addition to the above mechanism, the removal mechanism of Cr(VI) by LDH-CAC@1 may also be affected by pH (Sengupta 1984). At low pH, Cr(VI) in solution is mainly in the form of $HCrO_4^-$ and $Cr_2O_7^{2-}$ anions. According to the pH_{pzc} analysis of LDH-CAC@1, its surface carries a large number of positive charges, so it can also adsorb Cr(VI) by electrostatic attraction (Khitous et al. 2016). The removal mechanism is shown in Fig. 10.

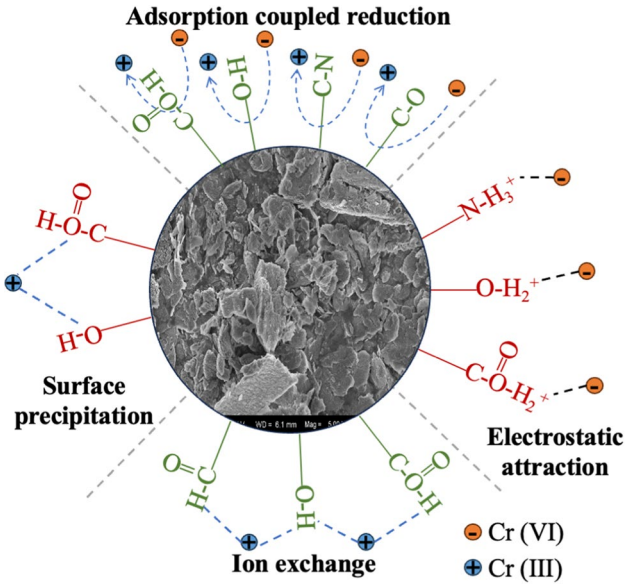

Fig. 10 The removal mechanisms of Cr(VI) by LDH-CAC@1

Effects of coexisting ions on the removal of Cr(VI)

Several coexisting ions such as Mg^{2+}, Ca^{2+}, SO_4^{2-}, PO_4^{3-}, and Cl^- (the ion concentration is 5 mM) are used to investigate the effect of coexisting ions on the Cr(VI) removal performance of LDH-CAC@1. Their effects on the Cr(VI) removal performance are shown in Fig. 11a. The difference in Cr(VI) removal efficiency is very small with the addition of Mg^{2+} and Ca^{2+}, which decreases by only 0.0048%, and 3.76%, respectively. The reduction in removal efficiency is probably due to the competitive effect of metal ions on active sites and functional groups. For anions, PO_4^{3-} and Cl^- had a smaller effect, with a decrease in Cr(VI) removal efficiency of 3.87% and 6.14%, respectively. The decrease is due to the involvement of PO_4^{3-}, and Cl^- in the electrostatic attraction as well as in the anion exchange process. For SO_4^{2-}, a more significant decrease in the Cr(VI) removal efficiency is observed. This is attributed to the fact that SO_4^{2-} and CrO_4^{2-} have similar specific structures and charge densities. As the whole, the impact of coexisting ions on Cr(VI) removal efficiency is small, indicating that LDH-CAC@1 can be used to treat industrial wastewater from different sources.

Reusability

To assess the reusability of LDH-CAC@1, regeneration and reuse performance studies are carried out. Alkali solutions can be used to desorb Cr(VI) by weakening the electrostatic

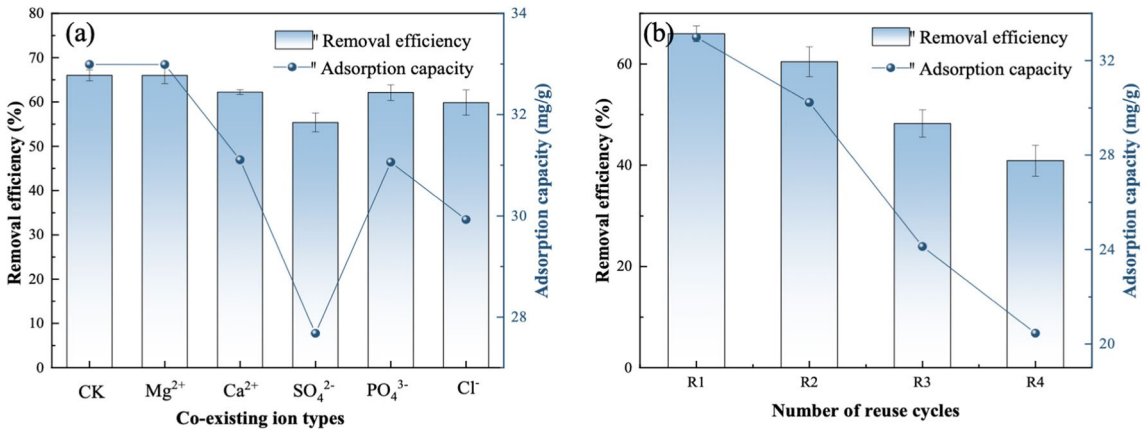

Fig. 11 Effect of coexisting ions towards Cr(VI) removal performance of LDH-CAC@1 (**a**) and reusability performance of LDH-CAC@1 after regeneration (**b**)

Table 6 Comparison of adsorption equilibrium time and maximum adsorption capacity of different adsorbents for Cr(VI) removal

Adsorbents	Adsorption equilibrium time (min)	Maximum adsorption capacity (mg/g)	Reference
BC@EDTA-LDH	1440	38	Huang et al. (2019)
MgAl-LDH/bentonite composites	1380	40	De Geest et al. (2023)
LDH-AL microspheres	–	17	Li et al. (2023)
Ni–Fe-CO_3 LDH	~30	6.1	Ahmed et al. (2023)
PDA/MgAl-LDH	~600	87	Ren et al. (2022b)
FeS/LDH	-	147.7	Zhang et al. (2022)
Magnetic $MnFe_2O_4$/ZnFe-LDH	~150	49.03	Huang et al. (2022)
Mg/Al LDH@mordenite	360	57.45	Dang et al. (2022)
LDH-CAC@1	**~10**	**116.7**	**This work**

attraction between the adsorbent and oxygen anion (Blaisi et al. 2018). Therefore, 0.1M NaOH is used for the desorption of LDH-CAC@1 composite in this work. Figure 11b presents the adsorption–desorption cycle of Cr(VI) on LDH-CAC@1. The results show that the removal of Cr(VI) decreases from 65.99 to 40.89% in three cycles. The reusability represents the excellent performance of LDH-CAC@1 for the removal of oxygen anion pollutants from water.

Comparison with other adsorbent for Cr(VI) removal

Table 6 summarizes the comparison of recent adsorbents prepared with LDH as a support material for Cr(VI) removal. Zhang et al. prepared FeS/LDH composites modified with $FeCl_2$ and Na_2S and reported a maximum adsorption capacity of 147.7 mg/g (Zhang et al. 2022). However, they do not address the regeneration and reuse of the adsorbent. Regenerability is a crucial aspect in practical engineering applications, since it can reduce engineering costs and greatly expand the application range of adsorbents. Meanwhile, the adsorption rate is vitally important for the removal of pollutants. It is found that the adsorbents listed in Table 6 have a longer adsorption equilibrium time, requiring up to 30 min to reach adsorption equilibrium. In contrast, LDH-CAC@1 not only has better removal performance and recyclability, but also can achieve adsorption equilibrium in a much shorter time. The above indicates that LDH-CAC@1 is a promising adsorbent for the removal of pollutants in wastewater.

Conclusion

In this study, LDH-CAC@1 composite is synthesized using MgAl-LDH and CAC by a two-step hydrothermal method. The adsorption capacity for Cr(VI) and the potential adsorption mechanism are explored. The results show that the maximum adsorption of Cr(VI) on the LDH-CAC@1 is 116.7 mg/g and the adsorption equilibrium is reached within 10 min. The main removal mechanisms are adsorption coupled reduction, ion exchange, surface precipitation, and electrostatic attraction. Furthermore, the reusability exhibits that LDH-CAC@1 still has superior removal performance within 3 cycles. Therefore, it is feasible that LDH-CAC composite can be used for the removal of heavy metal oxyanions in industrial wastewater treatment.

Author contribution All authors contributed to the study's design. Yunfeng Xu provided conceptualization and funding acquisition. Material preparation, data collection, and analysis were performed by Shijie Zhang. Ying Sun, Zexu Wang, and Chuyin Liu contributed to the draft of the manuscript and analysis. All authors read and approved the final manuscript.

Funding This work was supported by projects of the National Natural Science Foundation of China (21107067).

Data availability All data generated or analyzed during this study are included in this article.

Declarations

Competing interests The authors declare no competing interests.

Ethics approval and consent to participate Not applicable.

Consent for publication Not applicable.

References

Ahmed IM, Abd-Elhamid AI, Aly AA, Brase S, Nayl AA (2023) Synthesis of Ni-Fe-CO_3 layered double hydroxide as effective adsorbent to remove Cr(VI) and ARS-dye from aqueous media. Environ Technol Innov 31:103214. https://doi.org/10.1016/j.eti.2023.103214

Ali W, Zhang H, Mao K, Shafeeque M, Aslam MW, Yang XF, Zhong L, Feng XB, Podgorski J (2022) Chromium contamination in paddy soil-rice systems and associated human health risks in Pakistan. Sci Total Environ 826:153910. https://doi.org/10.1016/j.scitotenv.2022.153910

Bhuvaneswari K, Palanisamy G, Sivashanmugan K, Pazhanivel T, Maiyalagan T (2021) ZnO nanoparticles decorated multiwall carbon

nanotube assisted ZnMgAl layered triple hydroxide hybrid photocatalyst for visible light-driven organic pollutants removal. J Environ Chem Eng 9:104909. https://doi.org/10.1016/j.jece.2020.104909

Blaisi NI, Zubair M, Ihsanullah AS, Kazeem TS, Manzar MS, Al-Kutti W, Al Harthi MA (2018) Date palm ash-MgAl-layered double hydroxide composite: sustainable adsorbent for effective removal of methyl orange and eriochrome black-T from aqueous phase. Environ Sci Pollut Res 25:34319–34331. https://doi.org/10.1007/s11356-018-3367-2

Dang VM, Nguyen VD, Van HT, Nguyen VQ, Nguyen TN, Nghiem LD (2022) Removal of Cr(VI) and Pb(II) from aqueous solution using Mg/Al layered double hydroxides-mordenite composite. Sep Sci Technol 57:2432–2445. https://doi.org/10.1080/01496395.2022.2070500

De Geest M, Michielsen B, Ciocarlan RG, Cool P, Seftel EM (2023) Structured LDH/bentonite composites for chromium removal and recovery from aqueous solutions. Molecules 28:4879. https://doi.org/10.3390/molecules28124879

Dong YC, Kong XR, Luo XS, Wang HT (2022) Adsorptive removal of heavy metal anions from water by layered double hydroxide: A review. Chemosphere 303:134685. https://doi.org/10.1016/j.chemosphere.2022.134685

Extremera R, Pavlovic I, Perez MR, Barriga C (2012) Removal of acid orange 10 by calcined Mg/Al layered double hydroxides from water and recovery of the adsorbed dye. Chem Eng J 213:392–400. https://doi.org/10.1016/j.cej.2012.10.042

Fang KL, Chen MF, Chen JZ, Tian QH, Wong CP (2019) Cotton stalk-derived carbon fiber@Ni-Al layered double hydroxide nanosheets with improved performances for supercapacitors. Appl Surf Sci 475:372–379. https://doi.org/10.1016/j.apsusc.2019.01.002

Fang QZ, Ye SJ, Yang HL, Yang KH, Zhou JW, Gao Y, Lin QY, Tan XF, Yang ZZ (2021) Application of layered double hydroxide-biochar composites in wastewater treatment: recent trends, modification strategies, and outlook. J Hazard Mater 420:126595. https://doi.org/10.1016/j.jhazmat.2021.126569

Gao MK, Xu DH, Gao YH, Chen G, Zhai RQ, Huang XD, Xu XM, Wang J, Yang X, Liu GY (2021) Mussel-inspired triple bionic adsorbent: facile preparation of layered double hydroxide@polydopamine@metal-polyphenol networks and their selective adsorption of dyes in single and binary systems. J Hazard Mater 420:126609. https://doi.org/10.1016/j.jhazmat.2021.126609

Gao X, Peng YT, Guo LL, Wang Q, Guan CY, Yang F, Chen Q (2020) Arsenic adsorption on layered double hydroxides biochars and their amended red and calcareous soils. J Environ Manage 271. https://doi.org/10.1016/j.jenvman.2020.111045

Gholami P, Dinpazhoh L, Khataee A, Hassani A, Bhatnagar A (2020a) Facile hydrothermal synthesis of novel Fe-Cu layered double hydroxide/biochar nanocomposite with enhanced sonocatalytic activity for degradation of cefazolin sodium. J Hazard Mater 381:120742. https://doi.org/10.1016/j.jhazmat.2019.120742

Gholami P, Khataee A, Soltani RDC, Dinpazhoh L, Bhatnagar A (2020b) Photocatalytic degradation of gemifloxacin antibiotic using Zn-Co-LDH@biochar nanocomposite. J Hazard Mater 382:121070. https://doi.org/10.1016/j.jhazmat.2019.121070

Gong XM, Huang DL, Liu YG, Zeng GM, Wang RZ, Wan J, Zhang C, Cheng M, Qin X, Xue WJ (2017) Stabilized nanoscale zerovalent iron mediated cadmium accumulation and oxidative damage of Boehmeria nivea (L.) Gaudich cultivated in cadmium contaminated sediments. Environ Sci Technol 51:11308–11316. https://doi.org/10.1021/acs.est.7b03164

Gossuin Y, Hantson AL, Vuong QL (2020) Low resolution benchtop nuclear magnetic resonance for the follow-up of the removal of Cu^{2+} and Cr^{3+} from water by amberlite IR120 ion exchange resin. J Water Process Eng 33. https://doi.org/10.1016/j.jwpe.2019.101024

He C, Lin HL, Dai LL, Qiu RL, Tang YT, Wang YP, Duan PG, Ok YS (2020) Waste shrimp shell-derived hydrochar as an emergent material for methyl orange removal in aqueous solutions. Environ Int 134:105340. https://doi.org/10.1016/j.envint.2019.105340

Huang DL, Liu CH, Zhang C, Deng R, Wang RZ, Xue WJ, Luo H, Zeng GM, Zhang Q, Guo XY (2019) Cr(VI) removal from aqueous solution using biochar modified with Mg/Al-layered double hydroxide intercalated with ethylenediaminetetraacetic acid. Bioresour Technol 276:127–132. https://doi.org/10.1016/j.biortech.2018.12.114

Huang CX, Tang CC, Wu QQ, Zhu Q (2022) Magnetic $MnFe_2O_4$/ZnFe-LDH for enhanced phosphate and Cr (VI) removal from water. Environ Sci Pollut Res 29:59224–59234. https://doi.org/10.1007/s11356-022-20049-9

Hudcová B, Fein JB, Tsang DCW, Komárek M (2022): Mg-Fe LDH-coated biochars for metal(loid) removal: surface complexation modeling and structural change investigations. Chem Eng J 432. https://doi.org/10.1016/j.cej.2021.134360

Jia G, Hu YF, Qan QF, Yao YF, Zhang SY, Li ZS, Zou ZG (2016) Formation of hierarchical structure composed of (Co/Ni)Mn-LDH nanosheets on MWCNT backbones for efficient electrocatalytic water oxidation (vol 8, pg 14527, 2016). ACS Appl Mater Interfaces 8:22744–22744. https://doi.org/10.1021/acsami.6b09564

Khitous M, Salem Z, Halliche D (2016) Effect of interlayer anions on chromium removal using Mg-Al layered double hydroxides: kinetic, equilibrium and thermodynamic studies. Chin J Chem Eng 24:433–445. https://doi.org/10.1016/j.cjche.2015.11.018

Li ZH, Zhang XX, Chen JY, Fang X, Yuan WY, Yu JX, Qiu XH (2023) Preparing of layered double hydroxide- alginate microspheres for Cr (VI)-contaminated soil remediation. Colloids Surface A 658:130655. https://doi.org/10.1016/j.colsurfa.2022.130655

Liang QY, Pan Y, Zhang D, Lue T, Zhao HT, Zhang Y (2023) Preparation of bichar/layered double hydroxide@alginate aerogel as a highly efficient adsorbent for Cu^{2+} and Cd^{2+}. J Appl Polym Sci 140:1–12. https://doi.org/10.1002/app.53361

Lv D, Liu Y, Zhou JS, Yang KL, Lou ZM, Baig SA, Xu XH (2018) Application of EDTA-functionalized bamboo activated carbon (BAC) for Pb(II) and Cu(II) removal from aqueous solutions. Appl Surf Sci 428:648–658. https://doi.org/10.1016/j.apsusc.2017.09.151

Nayak S, Parida KM (2019) Deciphering Z-scheme charge transfer dynamics in heterostructure NiFe-LDH/N-rGO/g-C3N4 nanocomposite for photocatalytic pollutant removal and water splitting reactions. Sci Rep 9:2458. https://doi.org/10.1038/s41598-019-39009-4

Peng XM, Wang M, Hu FP, Qiu FX, Zhang T, Dai HL, Cao Z (2018) Multipath fabrication of hierarchical CuAl layered double hydroxide/carbon fiber composites for the degradation of ammonia nitrogen. J Environ Manage 220:173–182. https://doi.org/10.1016/j.jenvman.2018.05.037

Ren SQ, Wang YC, Han ZJ, Zhang QW, Cui CW (2022b) Synthesis of polydopamine modified MgAl-LDH for high efficient Cr(VI) removal from wastewater. Environ Res 215:114191. https://doi.org/10.1016/j.envres.2022.114191

Ren SQ, Wang YC, Han ZJ, Zhang QW, Cui CW (2022a) Synthesis of polydopamine modified MgAl-LDH for high efficient Cr(VI) removal from wastewater. Environ Res 215 https://doi.org/10.1016/j.envres.2022.114191

Sengupta AKZ (1984) Chromate ion-exchanges study for cooling water (recovery). University of Houston, Texas

Shim J-W, Park S-J, Ryu S-K (2001) Effect of modification with HNO3 and NaOH on metal adsorption by pitch-based activated carbon fibers. Carbon 39:1635–1642. https://doi.org/10.1016/S0008-6223(00)00290-6

Sirajudheen P, Karthikeyan P, Meenakshi S (2020) Mechanistic performance of organic pollutants removal from water using Zn/

Al layered double hydroxides imprinted carbon composite. Surf Interfaces 20:100581. https://doi.org/10.1016/j.surfin.2020.100581

Soleimani H, Sharafi K, Parian JA, Jaafari J, Ebrahimzadeh G (2023) Acidic modification of natural stone for Remazol Black B dye adsorption from aqueous solution- central composite design (CCD) and response surface methodology (RSM). Helyon 9:e14743. https://doi.org/10.1016/j.heliyon.2023.e14743

Srivastava A, Gupta B, Majumder A, Gupta AK, Nimbhorkar SK (2021) A comprehensive review on the synthesis, performance, modifications, and regeneration of activated carbon for the adsorptive removal of various water pollutants. J Environ Chem Eng 9:106177. https://doi.org/10.1016/j.jece.2021.106177

Tran HN, Nguyen DT, Le GT, Tomul F, Lima EC, Woo SH, Sarmah AK, Nguyen HQ, Nguyen PT, Nguyen DD, Nguyen TV, Vigneswaran S, Vo DVN, Chao HP (2019) Adsorption mechanism of hexavalent chromium onto layered double hydroxides-based adsorbents: a systematic in-depth review. J Hazard Mater 373:258–270. https://doi.org/10.1016/j.jhazmat.2019.03.018

Wang S, Gao B, Li Y, Zimmerman AR, Cao X (2016) Sorption of arsenic onto Ni/Fe layered double hydroxide (LDH)-biochar composites. RSC Adv 6:17792–17799. https://doi.org/10.1039/C5RA17490B

Wang RZ, Huang DL, Liu YG, Zhang C, Lai C, Zeng GM, Cheng M, Gong XM, Wan J, Luo H (2018) Investigating the adsorption behavior and the relative distribution of Cd^{2+} sorption mechanisms on biochars by different feedstock. Bioresour Technol 261:265–271. https://doi.org/10.1016/j.biortech.2018.04.032

Wang LW, Hou DY, Cao YN, Ok YS, Tack FMG, Rinklebe J, O'Connor D (2020) Remediation of mercury contaminated soil, water, and air: a review of emerging materials and innovative technologies. Environ Int 134:105281. https://doi.org/10.1016/j.envint.2019.105281

Wang X, Cheng B, Zhang LY, Yu JG, Normatov I (2022) Adsorption performance of tetracycline on NiFe layered double hydroxide hollow microspheres synthesized with silica as the template. J Colloid Interface Sci 627:793–803. https://doi.org/10.1016/j.jcis.2022.07.063

Wei SC, Li DT, Huang Z, Huang YQ, Wang F (2013) High-capacity adsorption of Cr(VI) from aqueous solution using a hierarchical porous carbon obtained from pig bone. Bioresour Technol 134:407–411. https://doi.org/10.1016/j.biortech.2013.02.040

Xue WJ, Huang DL, Zeng GM, Wan J, Zhang C, Xu R, Cheng M, Deng R (2018) Nanoscale zero-valent iron coated with rhamnolipid as an effective stabilizer for immobilization of Cd and Pb in river sediments. J Hazard Mater 341:381–389. https://doi.org/10.1016/j.jhazmat.2017.06.028

Yang SY, Zhao J, Chang SX, Collins C, Xu JM, Liu XM (2019) Status assessment and probabilistic health risk modeling of metals accumulation in agriculture soils across China: A synthesis. Environ Int 128:165–174. https://doi.org/10.1016/j.envint.2019.04.044

Yaseen M, Maria, Farooq MU, Ahmad W, Subhan F (2021) Fabrication of rGO-CuO and/or Ag_2O nanoparticles incorporated polyvinyl acetate based mixed matrix membranes for the removal of Cr^{6+} from anti-corrosive paint industrial wastewater. J Environ Chem Eng 9:105151. https://doi.org/10.1016/j.jece.2021.105151

Ye ZX, Yin XB, Chen LF, He XY, Lin ZM, Liu CC, Ning SY, Wang XP, Wei YZ (2019) An integrated process for removal and recovery of Cr(VI) from electroplating wastewater by ion exchange and reduction-precipitation based on a silica-supported pyridine resin. J Cleaner Prod 236:117631. https://doi.org/10.1016/j.jclepro.2019.117631

Yin L, Wang PY, Wen T, Yu SJ, Wang XX, Hayat T, Alsaedi A, Wang XK (2017) Synthesis of layered titanate nanowires at low temperature and their application in efficient removal of U(VI). Environ Pollut 226:125–134. https://doi.org/10.1016/j.envpol.2017.03.078

Yue XY, Liu WZ, Chen ZL, Lin Z (2017) Simultaneous removalofCu(II) and Cr(VI) by Mg-Al-Cl layered double hydroxide and mechanism insight. J Environ Sci 53:16–26. https://doi.org/10.1016/j.jes.2016.01.015

Zhang Y, Du DF, Li XJ, Sun HM, Lo L, Bai P, Xing W, Xue QZ, Yan ZF (2017) Electrostatic self-assembly of sandwich-like CoAl-LDH/polypyrrole/graphene nanocomposites with enhanced capacitive performance. ACS Appl Mater Interfaces 9:31699–31709. https://doi.org/10.1021/acsami.7b04792

Zhang SS, Zhang WH, Wan YZ (2022) Adsorption and reduction of aqueous Cr by FeS-modified Fe-Al layered double hydroxide. Sustainability 14:21. https://doi.org/10.3390/su14010021

Zhao FJ, Ma YB, Zhu YG, Tang Z, McGrath SP (2015) Soil contamination in China: current status and mitigation strategies. Environ Sci Technol 49:750–759. https://doi.org/10.1021/es5047099